Quantum-classical correspondence in localization of eigenstates for a system having mixed-type classical dynamics

Sang Wook Kim and Hai-Woong Lee
Department of Physics, Korea Advanced Institute of Science and Technology, Taejon 305-338, Korea
(Received 29 September 1998; revised manuscript received 29 December 1998)

We have examined the localization properties of quantum eigenstates for a system having mixed-type classical dynamics. Emphasis is given to the structure of eigenfunctions and the local spectral density of states. The nature of strongly localized eigenstates can be explained by considering the corresponding classical motion on the Kolmogorov-Arnold-Moser tori. The weak localization of nearly delocalized eigenstates is not a quantum effect as is dynamical localization but a consequence of classical dynamics.
[S1063-651X(99)15605-8]

PACS number(s): 05.45.−a

I. INTRODUCTION

The quantum-mechanical behavior of systems that are chaotic in the classical limit has been the subject of considerable recent interest [1–3]. One major modification that quantum mechanics introduces to the classical picture of deterministic chaos is the suppression of chaotic diffusion, a phenomenon usually referred to as dynamical localization (DL). Since it was first observed in numerical simulations of the kicked rotator model [4], this striking quantum phenomenon, a dynamical version of Anderson localization in solids [5], has been under intense investigation. In particular, theoretical and experimental investigations of microwave ionization of Rydberg atoms [6–10] and recently of momentum transfer in cold atoms [11–14] have provided evidence for the appearance of DL.

It should be noted, however, that investigations conducted up to now have been limited to DL occurring in time-driven systems. Quantum calculations performed in the past have treated the external driving force classically and should strictly speaking be categorized as semiclassical treatments. The question still remains whether the existence of DL has been confirmed by fully quantum calculations. Recently, it has been shown [15] that DL also appears in a nearly circular stadium billiard. From the estimate of the localization length in the angular momentum space, the authors of Ref. [15] found that the statistics of neighboring level spacing could change from Wigner-Dyson to Poisson when the energy range is varied. To our knowledge this is the first evidence for DL in a conservative Hamiltonian system.

How one should approach the question of localization in conservative Hamiltonian systems is not immediately clear; since energy is conserved in both classical and quantum systems, we must follow the time evolution only on the energy hypersurface. In classical mechanics this is easily realized by considering the dynamics on the energy hypersurface, but in quantum mechanics the only states with fixed energy are eigenstates unless the spectrum is degenerate [16]. This is resolved by considering the flow between phase-space localized states (usually coherent states). Another approach is to investigate the localization properties of eigenstates for a typical conservative Hamiltonian or random matrix ensemble [17], where in the latter the main attention is paid to the banded random matrices (BRM) ensemble [18,19]. Casati *et al*. introduced the ergodicity parameter λ depending on both the band width and average localization length, which plays an important role in determining the localization properties in the BRM [20]. When it is large, the eigenfunctions (EF's) of BRM become ergodic, i.e., delocalized over the whole energy shell. In the opposite case, however, they appear to be localized in the eigenstate space of the unperturbed Hamiltonian. When quantum localization occurs, the EF's were shown to be typically narrow and solid with centers randomly scattered within a semicircle energy shell, while the local spectral density of states (LSDS) is extended over the whole shell, but is sparse.

Generic conservative Hamiltonian systems exhibit mixed-type dynamics; the regular Kolmogorov-Arnold-Moser (KAM) tori and irregular chaotic trajectories coexist in phase space. In 1973 Percival conjectured that, in the semiclassical limit, the spectrum of a generic dynamical system consists of two parts with strong contrasting properties: a regular and an irregular part [21–23]. Bohigas *et al*. [24] achieved a systematic separation of eigenstates of two coupled quartic oscillators into a regular and an irregular group. The separation was based on the observation that the levels associated with quantized tori appear as quasidegenerate doublets in the spectrum of systems having discrete symmetries. By studying the regular and irregular spectra independently after the separation, they showed that Percival's scheme works well.

In this paper we address the issue of quantum localization in a typical generic conservative Hamiltonian system, namely, the Pullen-Edmond system [25]. We look in particular for quantum-classical correspondence (or noncorrespondence) by investigating the relation between the localization properties of LSDS and those of EF's. Our model system and its Hamiltonian structure are described in Sec. II. In Sec. III localization properties of LSDS and EF's are investigated in detail. For our model system the structure of LSDS can easily be interpreted by investigating classical dynamics. We show eventually that a strong quantum-classical correspondence exists for both EF's showing strong localization and EF's exhibiting delocaliztion or weak localization [26]. Finally, concluding remarks are given in Sec. V.

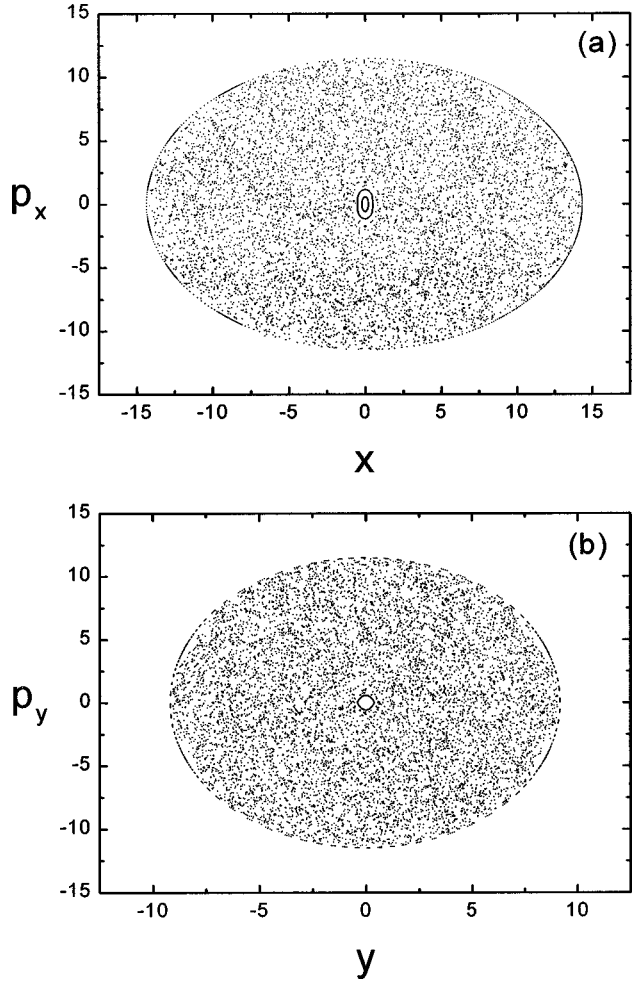

FIG. 1. The classical Poincaré surfaces of section of the Pullen-Edmond system defined by Eq. (1) for the case $m=1$, $\omega_x=0.8$, $\omega_y=1.25$, $\lambda=0.3$, and $\lambda E=19.75$ in an arbitrary unit system. (a) The x-p_x plot drawn at $y=0$ and $p_y>0$. (b) The y-p_y plot drawn at $x=0$ and $p_x>0$.

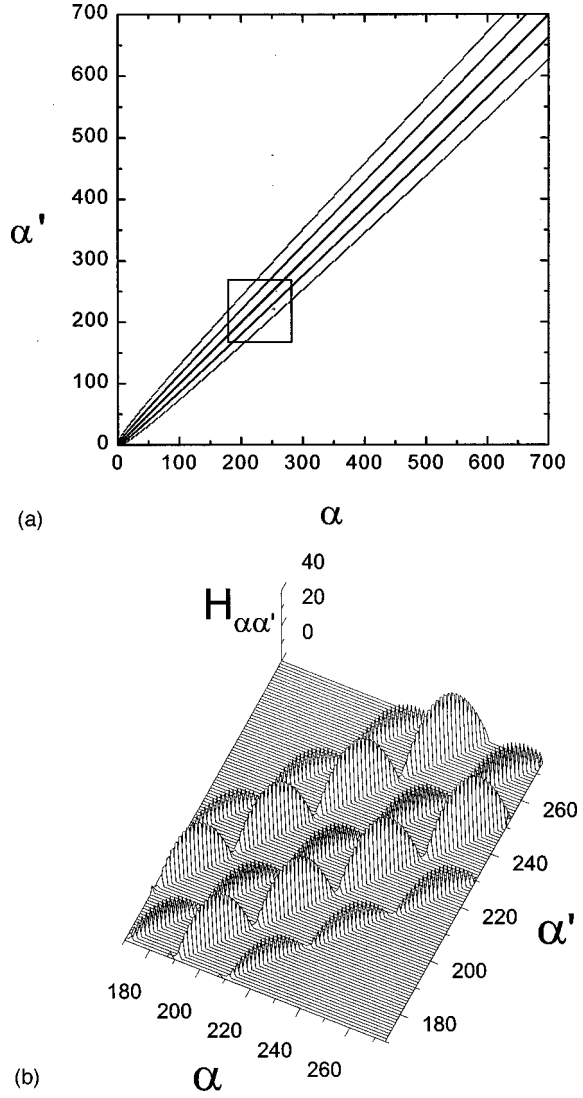

FIG. 2. (a) Structure of the Hamiltonian matrix $H_{\alpha,\alpha'}$ in terms of the quantum numbers α, α' of the eigenstates of the unperturbed Hamiltonian H_0. $H_{\alpha,\alpha'}$ is nonzero only along the lines. (b) The magnitude of the matrix elements represented by the square in (a). The diagonal values are set to zero for clarity.

II. MODEL SYSTEM AND HAMILTONIAN STRUCTURE

The system we consider is the Pullen-Edmond system, a two-dimensional autonomous Hamiltonian system representing two nonlinearly coupled simple harmonic oscillators. The Hamiltonian for the system is given by

$$H(x,p_x,y,p_y)=\frac{1}{2m}(p_x^2+p_y^2)+\frac{m}{2}(\omega_x^2x^2+\omega_y^2y^2)+\frac{\lambda}{2}x^2y^2$$

$$\equiv H_0+\frac{\lambda}{2}x^2y^2. \tag{1}$$

For our computation we fix $m=1$, $\omega_x=0.8$, $\omega_y=1.25$, and $\lambda=0.3$ in an arbitrary unit system. We note that the transformation $\lambda\rightarrow\lambda'=\lambda/\gamma$ ($\gamma=$ const) does not alter the dynamical nature of the system if the transformation $x\rightarrow x'=\sqrt{\gamma}x$, $y\rightarrow y'=\sqrt{\gamma}y$, $p_x\rightarrow p_x'=\sqrt{\gamma}p_x$, $p_y\rightarrow p_y'=\sqrt{\gamma}p_y$, and thus $E\rightarrow E'=\gamma E$ (E is the total energy) is performed simultaneously. The geometry of classical phase space is thus determined only by the product of λ and E. When the scaling parameter λE is small, many stable KAM tori originated from resonances between the two degrees of freedom exist in the chaotic region. As the parameter increases, however, most KAM tori are replaced by irregular trajectories and only small portions of the phase space remain stable. When the parameter exceeds approximately 12.0, nearly the entire phase space becomes irregular [27], except the region near the origin in which the coupling $\lambda x^2y^2/2$ is small and thus the trajectories remain regular (see Fig. 1).

We represent the total Hamiltonian H in terms of the eigenstates (n_x,n_y) of the unperturbed Hamiltonian H_0, where the matrix elements have the form

$$\langle n_x',n_y'|H|n_x,n_y\rangle=\{\hbar\omega_x(n_x+1/2)+\hbar\omega_y(n_y+1/2)\}\delta_{n_x',n_x}\delta_{n_y',n_y}+m\sqrt{\omega_x\omega_y}\lambda\{(2n_x+1)(2n_y+1)\delta_{n_x',n_x}\delta_{n_y',n_y}$$
$$+\sqrt{n_x(n_x-1)n_y(n_y-1)}\delta_{n_x',n_x-2}\delta_{n_y',n_y-2}+\sqrt{(n_x+1)(n_x+2)n_y(n_y-1)}\delta_{n_x',n_x+2}\delta_{n_y',n_y-2}$$
$$+(2n_x+1)\sqrt{n_y(n_y-1)}\delta_{n_x',n_x}\delta_{n_y',n_y-2}+\sqrt{n_x(n_x-1)(n_y+1)(n_y+2)}\delta_{n_x',n_x-2}\delta_{n_y',n_y+2}$$
$$+\sqrt{(n_x+1)(n_x+2)(n_y+1)(n_y+2)}\delta_{n_x',n_x+2}\delta_{n_y',n_y+2}+(2n_x+1)\sqrt{(n_y+1)(n_y+2)}\delta_{n_x',n_x}\delta_{n_y',n_y+2}$$
$$+(2n_y+1)\sqrt{n_x(n_x-1)}\delta_{n_x',n_x-2}\delta_{n_y',n_y}+(2n_y+1)\sqrt{(n_x+1)(n_x+2)}\delta_{n_x',n_x+2}\delta_{n_y',n_y}\}/16\hbar. \quad (2)$$

Due to the choice of different values of ω_x and ω_y, our system has the symmetry of the C_{2v} point group which has four irreducible representations referred to as A_1, A_2, B_1, and B_2 [28]. From now on we only consider the A_1 representation for which basis functions are even in both x and y. Our labeling of the basis, the eigenstates of H_0, uses a single quantum number α as indicated in Table I. These eigenstates can be divided conveniently into subgroups, each having the same value of (n_x+n_y).

Figure 2(a) shows the global structure of the matrix elements $H_{\alpha,\alpha'}$, whose band structure differs from those of the Wigner BRM and Ref. [29]. In particular we see from Fig. 2(b) that off-diagonal elements have a typical periodic structure. The off-diagonal matrix elements $H_{\alpha,\alpha'}$ are small when α and/or α' correspond to the edges of a subgroup of eigenstates associated with a small n_x or n_y, while they are large when α and α' correspond to the middle of a subgroup. This has a simple classical interpretation. The classical trajectories of a phase space point belonging to the edge states are probably regular, because a small $n_x(n_y)$ means a small coupling $\lambda x^2y^2/2$ and thus oscillation occurs predominantly along the $y(x)$ axis.

The periodic structure seen above can be better understood by examining the phase-space structure of the system. For this purpose we choose to use the Q function, i.e., the quantum phase-space distribution function in the coherent state representation [30,31]. The Q function best fits our purpose because it has the simplest structure among quantum distribution functions and still displays all the essential features of the states of the system. The Q function for an unperturbed eigenstate $|\alpha\rangle$ of our system characterized by the quantum numbers n_x and n_y is given by [31]

$$F^Q(x,p_x,y,p_y)=\frac{1}{(2\pi\hbar)^2 n_x!n_y!}\xi_x^{n_x}e^{-\xi_x}\xi_y^{n_y}e^{-\xi_y}, \quad (3)$$

where

$$\xi_x=\frac{m\omega_x x^2}{2\hbar}+\frac{p_x^2}{2\hbar m\omega_x} \quad (4)$$

and

$$\xi_y=\frac{m\omega_y y^2}{2\hbar}+\frac{p_y^2}{2\hbar m\omega_y}. \quad (5)$$

In Figs. 3(a) and 3(b) we plot $F^Q(x,p_x,y=0,p_y=\sqrt{2mE_{n_x,n_y}-p_x^2-m^2\omega_x^2x^2})$ for the $\alpha=65$ $(n_x=0,n_y=20)$ and $\alpha=60$ $(n_x=10,n_y=10)$ states, respectively, where we set $\hbar=1$ in an arbitrary unit system we adopt. The functions F^Q plotted in Figs. 3(a) and 3(b) may be considered as quantum Poincaré surfaces of section corresponding to the unperturbed eigenstates of $\alpha=65$ and $\alpha=60$. One can clearly see, by comparing Figs. 3(a) and 3(b) with Fig. 1(a), that the distribution of the $\alpha=60$ state is localized mostly at the classically chaotic region, while that of the $\alpha=65$ state is concentrated in the classical Kolmogorov-Arnold-Moser (KAM) island near the origin.

To gain further insight we consider the motion in the coordinate space. The classical KAM island near the origin in Fig. 1(a) corresponds to the straight line motion along the y axis indicated by the vertical line with arrows in Fig. 4. This motion may be considered as a classical representation of the $\alpha=65$ unperturbed eigenstate because this eigenstate with $n_x=0$ has no node along the x direction. We also show the density $|\psi(x,y)|^2$ of the wave function of the $\alpha=65$ state in the same figure.

III. LOCALIZATION OF EIGENSTATES

For our discussion of localization, we first find the unitary matrix U that diagonalizes the total Hamiltonian H,

$$U^\dagger HU=H_{\text{diagonal}}. \quad (6)$$

Denoting the matrix elements of U as c_m^α, where α and m refer, respectively, to the quantum numbers of the eigenstates of the unperturbed Hamiltonian H_0 and the total Hamiltonian H, the column vector $(c_m^1,c_m^2,c_m^3,\dots)$ represents the mth eigenstate $|m\rangle$ of H expressed in terms of the eigenstates of H_0 (i.e., the spectrum of the state $|m\rangle$), while the row vector $(c_1^\alpha,c_2^\alpha,c_3^\alpha,\dots)$ represents the αth eigen-

TABLE I. Labeling of eigenstates of H_0 belonging to the A_1 representation.

α	0	1	2	3	4	5	⋯	55	56	57	58	59	60	61	62	63	64	65	⋯
n_x	0	2	0	4	2	0	⋯	20	18	16	14	12	10	8	6	4	2	0	⋯
n_y	0	0	2	0	2	4	⋯	0	2	4	6	8	10	12	14	16	18	20	⋯

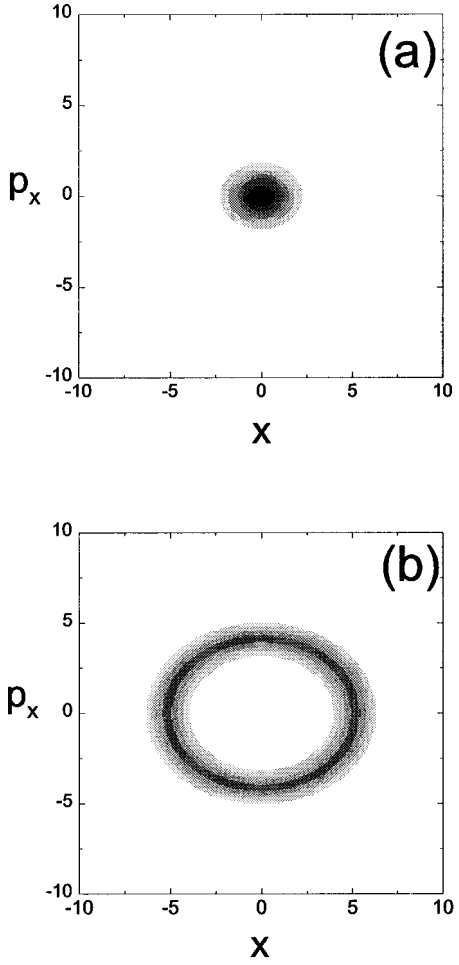

FIG. 3. Quantum Poincaré surfaces of section of the Q representation of (a) the $\alpha=65$ state and (b) the $\alpha=60$ state, which lie mostly in the regular and irregular regions of the classical Poincaré surfaces of section (Fig. 1), respectively. x and p_x are measured in arbitrary units.

state $|\alpha\rangle$ of H_0 expressed in terms of the eigenstates of H. The matrix elements c_m^α now contain all the information concerning the localization properties of the eigenstates.

A. Localization of LSDS

In this paper we adopt the inverse partition ratio (IPR) as the localization measure. The IPR of the unperturbed eigenstate $|\alpha\rangle$ is calculated from

$$L_{\mathrm{IPR}}(\alpha)=N\sum_{m=1}^{N}|c_m^\alpha|^4, \tag{7}$$

where N is the total number of eigenstates $|m\rangle$ of the total Hamiltonian H. In our actual calculation of $L_{\mathrm{IPR}}(\alpha)$, we have included in the sum only classically accessible states among all possible states $|m\rangle$. The number N in Eq. (7) can thus be considered as the number of classically accessible eigenstates $|m\rangle$, and it varies with α. $L_{\mathrm{IPR}}(\alpha)$ as defined by Eq. (7) can take a value as large as N when the state $|\alpha\rangle$ is most highly localized (i.e., when c_m^α is nonzero for only one particular value of m) and as small as 1 when the state $|\alpha\rangle$ is uniformly distributed (i.e., when $c_m^\alpha=1/\sqrt{N}$ for all m) [32,34].

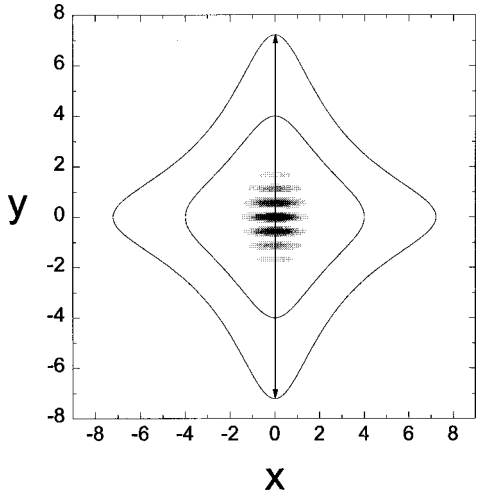

FIG. 4. Representation in the coordinate space. The line with arrows indicates the trajectory of the periodic orbit corresponding to the stable island. The density $|\psi(x,y)|^2$ of the $\alpha=65$ eigenfunction and the potential energy contour are also shown. x and y are measured in arbitrary units.

Figure 5 shows L_{IPR} of the unperturbed eigenstates which indicates clearly that the eigenstates $|\alpha\rangle$ belonging to the edges of each subgroup (i.e., those states with a small n_x or n_y) have large values of L_{IPR}. As explained in the previous section, these states correspond classically to regular trajectories around stable KAM tori and can thus be expected to exhibit strong localization. In order to emphasize the strong correlation between localization and the quantum numbers (n_x,n_y), we plot in Fig. 6 L_{IPR} versus $n_x/(n_x+n_y)$. Clearly, L_{IPR} is large when $n_x/(n_x+n_y)\approx 0$ (i.e., when $n_x\approx 0$) and when $n_x/(n_x+n_y)\approx 1$ (i.e., when $n_y\approx 0$). We note that the graph is not symmetric about $n_x/(n_x+n_y)=0.5$, because ω_x and ω_y are not the same.

B. Localization of EF

We also use IPR in order to investigate the localization properties of EF's. The IPR of an eigenstate $|m\rangle$ of the total Hamiltonian is given by

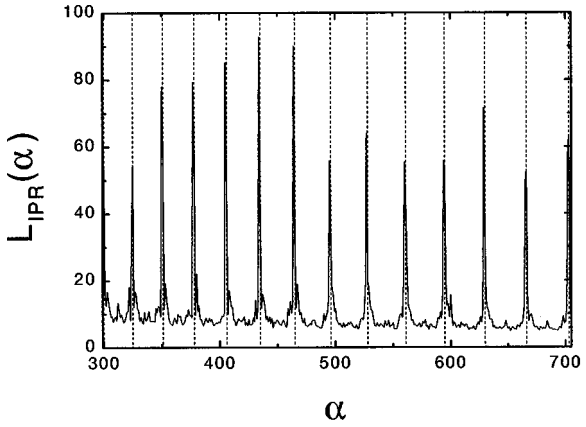

FIG. 5. L_{IPR} of LSDS for $300\leqslant\alpha\leqslant 700$. The positions of the eigenstates belonging to the edge of each subgroup are indicated by dashed lines.

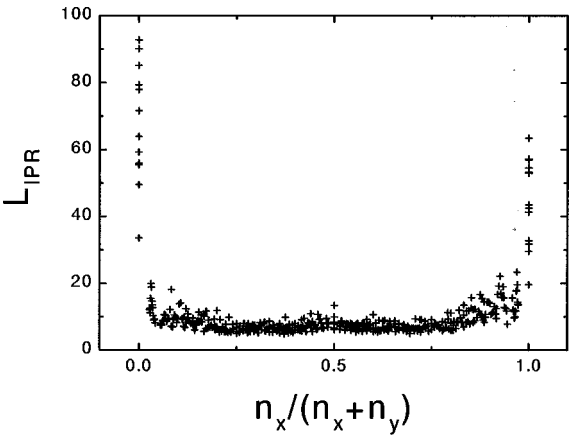

FIG. 6. L_{IPR} versus $n_x/(n_x+n_y)$ of LSDS.

$$L_{\mathrm{IPR}}(m)=N\sum_{\alpha=1}^{N}|c_m^{\alpha}|^4, \tag{8}$$

where N is now the total number of eigenstates $|\alpha\rangle$ of the unperturbed Hamiltonian H_0. We also consider only classically accessible states when calculatiing $L_{\mathrm{IPR}}(m)$ according to Eq. (8).

We choose EF's, arranged in ascending order of eigenenergy, from 300th to 700th, which correspond to the region $19.75\leqslant\lambda E\leqslant 32.57$. In this range of λE, almost the entire classical phase space is chaotic. Figure 7 shows L_{IPR} of these eigenstates. The distribution seen in Fig. 7 seems rather random, in contrast to the regular pattern of Fig. 5. This reflects the fact that for a system having mixed type classical dynamics, it is normally difficult to tell whether a given eigenstate $|m\rangle$ is associated with regular or irregular classical trajectories. Despite the difficulty, however, it can be seen from Fig. 7 that the eigenstates $|m\rangle$ can largely be divided into two groups, ''localized states'' characterized by large values of $L_{\mathrm{IPR}}(m)$ and ''delocalized states'' having small values of $L_{\mathrm{IPR}}(m)$. In Figs. 8(a) and 8(b), respectively, we show the spectrum of typical localized ($m=534$, $L_{\mathrm{IPR}}=220.5$) and delocalized ($m=535$, $L_{\mathrm{IPR}}=3.588$) states drawn in terms of the quantum number α of the unperturbed eigenstates. It should be noted that the ($m=535$) state of Fig. 8(b), although we call it a delocalized state to distinguish from a strongly localized state such as the ($m=534$) state of Fig. 8(a), is not completely delocalized, which we refer also to as weakly localized [26].

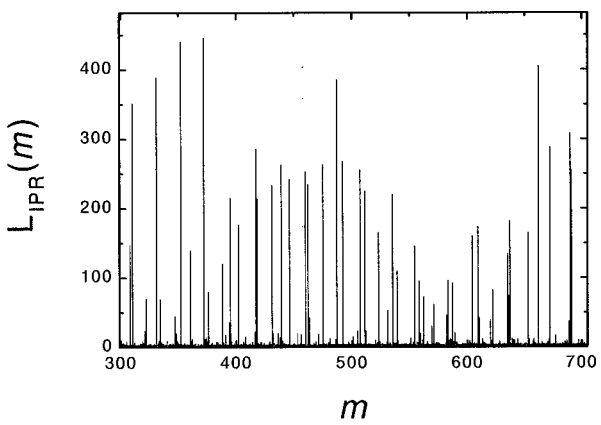

FIG. 7. L_{IPR} of EF's for $300\leqslant m\leqslant 700$.

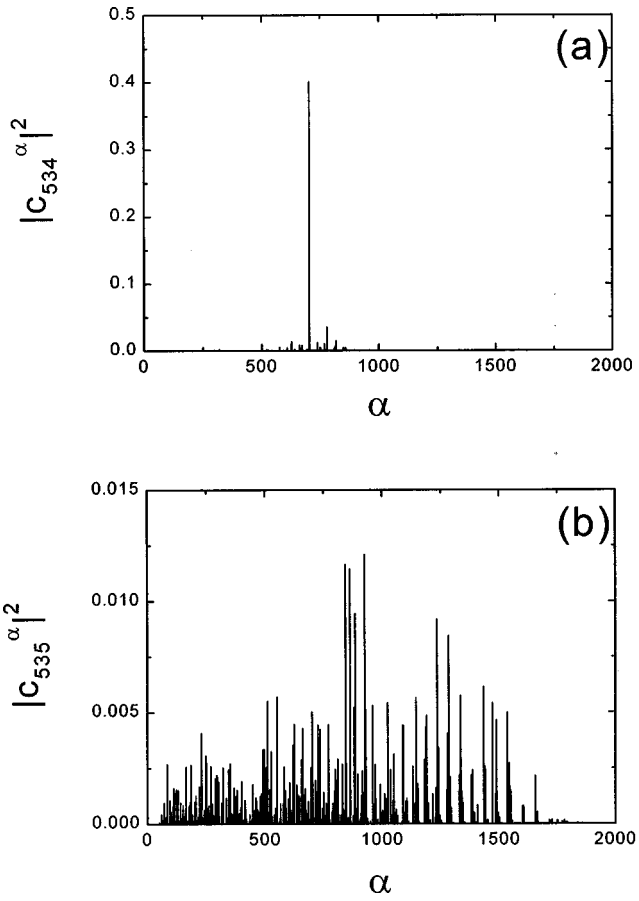

FIG. 8. (a) Spectrum of a typical localized EF for which $\lambda E=27.78$, $m=534$, and $L_{\mathrm{IPR}}(m)=220.5$. (b) Spectrum of a typical delocalized EF for which $\lambda E=27.81$, $m=535$, and $L_{\mathrm{IPR}}(m)=3.588$.

In order to investigate further the characteristics of the localized and delocalized states, we recast Fig. 8 into a two-dimensional shadow plot of the spectrum drawn in terms of the two quantum numbers n_x and n_y of the unperturbed eigenstates. The result is shown in Fig. 9, where the probability is indicated by the degree of darkness. It can be clearly seen that the localized ($m=534$) state has the probability distribution localized near $n_x=0$, whereas the delocalized ($m=535$) state shows a more or less randomly distributed probability.

It may be worthwhile to recall that although n_x and n_y are not good quantum numbers for the system described by the total Hamiltonian H, the mean values $\langle n_x\rangle$ and $\langle n_y\rangle$ can of course be defined and calculated for a given eigenstate $|m\rangle$ of H. In Fig. 10 we show $L_{\mathrm{IPR}}(m)$ plotted as a function of $\langle n_x\rangle/\langle n_x+n_y\rangle$. One can immediately see that a remarkable correspondence exists between Fig. 10 and Fig. 6. This correspondence between L_{IPR} of EF's and L_{IPR} of LSDS's is significant, because, as discussed earlier, the latter has a simple classical interpretation.

The physical characteristics of our localized and delocalized states can be best illustrated by looking at the statistical properties of eigenvalues [17,33] belonging to each group

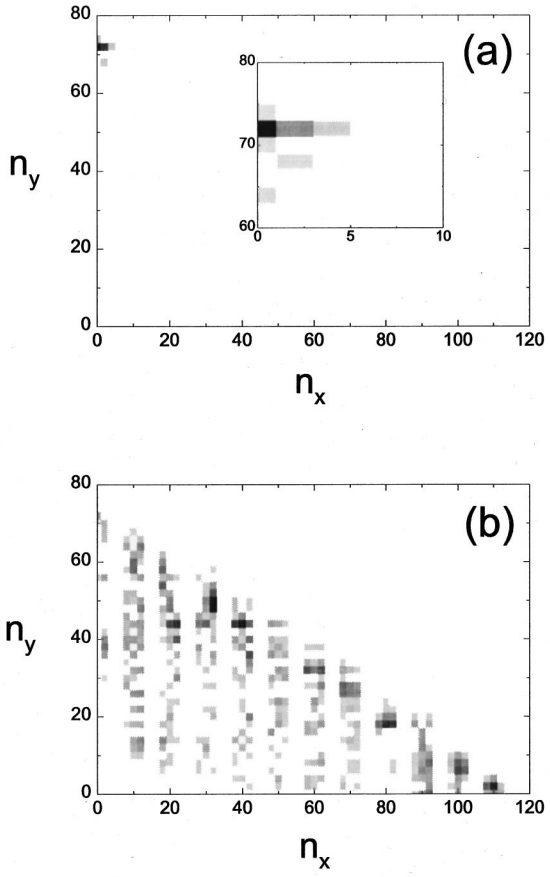

FIG. 9. Spectrum of (a) the localized ($m=534$) state and (b) the delocalized ($m=535$) state drawn as a function of n_x and n_y. The probability is indicated by the degree of darkness. The inset in (a) shows an expanded view of the spectrum of the localized ($m=534$) state.

separately in Percival's spirit [21]. We set the dividing line between the localized and delocalized states to be a somewhat arbitrary L_{IPR} value of 10; i.e., EF's with $L_{\mathrm{IPR}} \geqslant 10$ are considered as localized states and EF's with $L_{\mathrm{IPR}} < 10$ delocalized states. Our choice of the L_{IPR} value 10 has no particular physical significance. The results shown below are independent of this value, unless it is chosen unrealistically too large or too small. With our choice of $L_{\mathrm{IPR}}=10$, there are

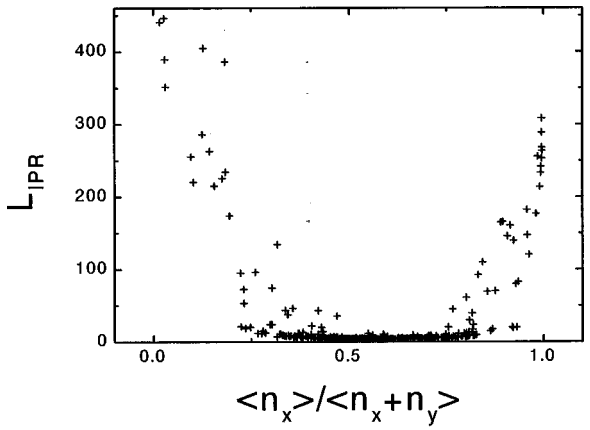

FIG. 10. L_{IPR} versus $\langle n_x\rangle/\langle n_x+n_y\rangle$ of EF's.

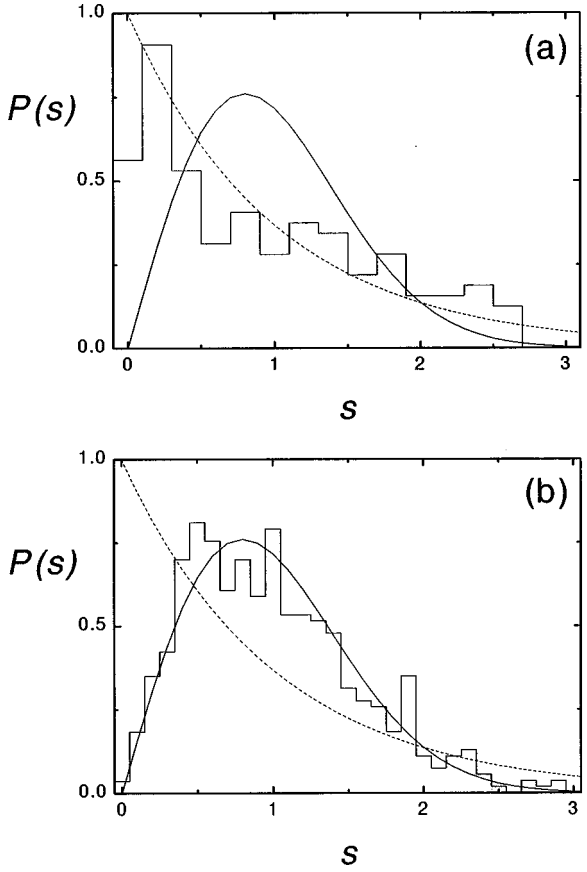

FIG. 11. Nearest neighbor level spacing distributions for (a) the localized eigenstates having values of L_{IPR} larger than 10 and (b) the delocalized eigenstates having values of L_{IPR} smaller than 10. The solid and the dashed curves represent the Wigner (GOE) distribution and the Poisson distribution, respectively.

161 localized states and 544 delocalized states within the range we consider. In Figs. 11(a) and 11(b) we show nearest-neighbor level spacing distributions for the localized and delocalized states, respectively. One can see that the level spacing distributions of the localized and delocalized states exhibit roughly Poisson-like behavior and Wigner-like behavior, respectively. For a closer look we show in Fig. 12 the

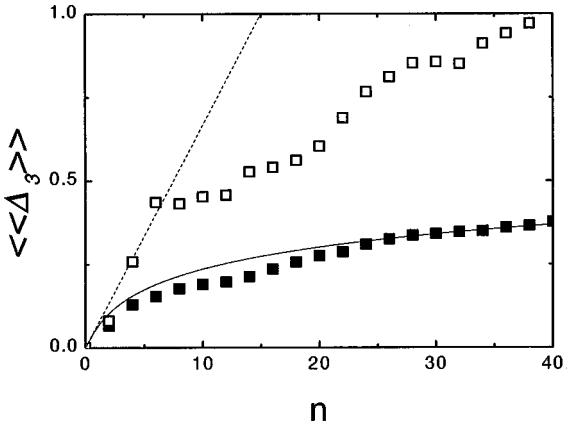

FIG. 12. Δ_3 statistics for the localized eigenstates (open squares) and the delocalized eigenstates (filled squares). The solid and the dashed curves represent the Wigner (GOE) distribution and the Poisson distribution, respectively.

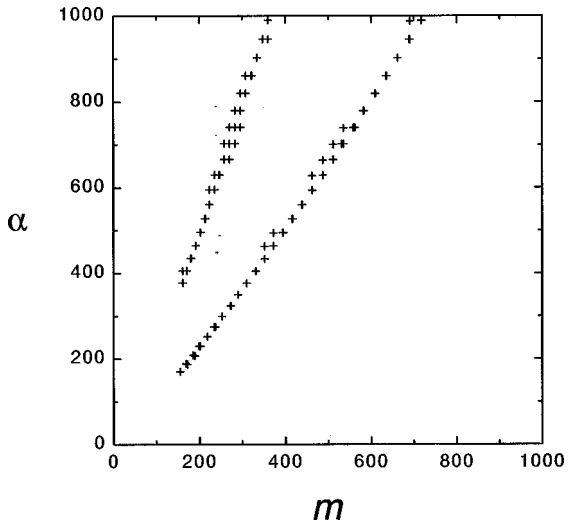

FIG. 13. The elements of the unitary matrix U having the absolute square value larger than 0.1.

Δ_3 statistics of the eigenvalues of the localized and delocalized states. It can be seen that the eigenvalues of the delocalized states follow the Wigner distribution fairly closely, while those of the localized states exhibit the behavior intermediate between the Poisson and Wigner distributions. We mention that the level spacing distribution and Δ_3 statistics of the entire eigenvalues of both the localized and delocalized states exhibit Wigner-like behavior.

Now we investigate the structure of the unitary matrix U. In Fig. 13 we show the matrix elements whose absolute square is greater than 0.1. We mention that 0.1 has no particular physical meaning. It is simply a fairly large number, because, if we assume a uniform distribution in both EF's and LSDS's, the values of the matrix elements would be equal to $1/N(\approx 0.001)$. Comparing Fig. 13 with Fig. 5 and with Fig. 7, it can be concluded that the quantum numbers α associated with large matrix elements of U coincide with the quantum numbers α associated with high $L_{\mathrm{IPR}}(\alpha)$, and similarly the quantum numbers m associated with large matrix elements of U coincide with the quantum numbers m associated with high $L_{\mathrm{IPR}}(m)$. This is another indication that the localization of EF's is directly linked to the localization of LSDS's which is in turn directly related to the localization of classical trajectories on the KAM tori. It is noted that the upper branch and the lower branch in Fig. 13 correspond to the localization of EF's along the x axis and the y axis in the coordinate space, respectively.

Finally we take a closer look at the localization properties of delocalized EF's having very small L_{IPR} ($\lesssim 3.5$). We have already seen from Fig. 8(b) that a typical delocalized eigenstate is not completely delocalized, rather it is weakly localized and sparse. In Fig. 14 we show the probability distributions of some delocalized EF's drawn as a function of the unperturbed energy E_0 calculated by both classical and quantum methods. To obtain the classical distribution, we first chose 50 sets of initial coordinates and momenta $(x_0, p_{x0}, y_0, p_{y0})$ on the constant total energy surface $E = E_m$, where E_m is the energy of the EF being considered. In order to assure that our initial points correspond to the delocalized EF, we first chose x_0 and p_{x0} randomly from the chaotic sea of Fig. 1(a) and set $y_0 = 0$. The p_{y0} value is then fixed by

$$\frac{1}{2m}(p_{x0}^2 + p_{y0}^2) + \frac{m}{2}\omega_x^2 x_0^2 = E_m . \tag{9}$$

For each set of initial points $(x_0, p_{x0}, y_0, p_{y0})$ so chosen, we then computed numerically classical trajectories to obtain $(x(t_n), p_x(t_n), y(t_n), p_y(t_n))$, where $t_n = n\Delta t$ and Δt is the time step for integration. At each t_n, we also computed $E_0(t_n)$ given by

$$E_0(t_n) = \frac{1}{2m}[p_x^2(t_n) + p_y^2(t_n)] + \frac{m}{2}[\omega_x^2 x^2(t_n) + \omega_y^2 y^2(t_n)]. \tag{10}$$

For our computation we chose $\Delta t = 0.001$ and $n = 1, 2, \ldots, 500\,000$ (i.e., the integration was carried out from $t = 0$ to $t = 500\,000\Delta t = 500$). Repeating the same procedure

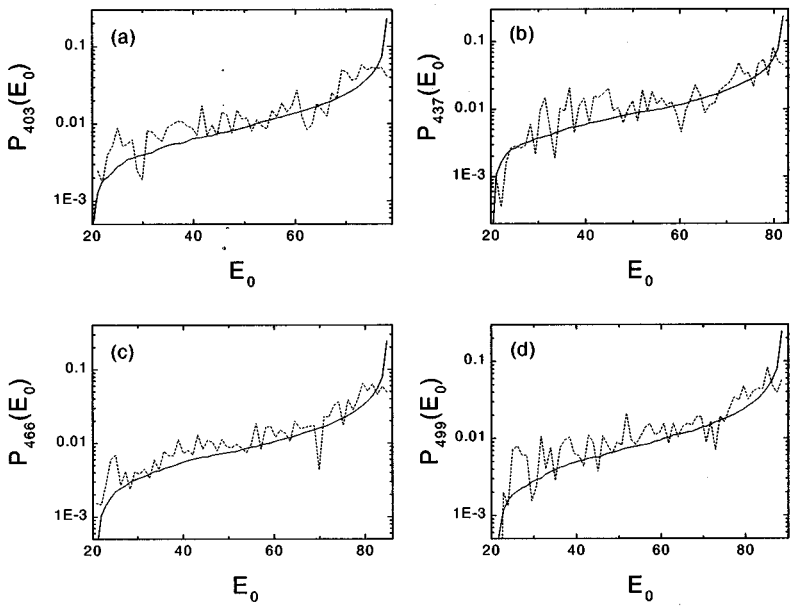

FIG. 14. Probability distributions of delocalized EF's in terms of the unperturbed energy E_0. The solid and the dashed curves correspond to classical and quantum distributions, respectively. The delocalized EF's are (a) $m = 403$ ($L_{\mathrm{IPR}} = 3.41$), (b) $m = 437$ ($L_{\mathrm{IPR}} = 3.45$), (c) $m = 466$ ($L_{\mathrm{IPR}} = 3.45$), and (d) $m = 499$ ($L_{\mathrm{IPR}} = 3.22$).

for all 50 sets of initial points, we collected a total of $500\,000\times 50=25\,000\,000$ values of E_0, from which the classical distribution shown in Fig. 12 was obtained. We note that the classical distribution computed as above is independent of the integration time step Δt and of the number of the trajectories. The corresponding quantum distribution is obtained by calculating

$$P_m(E_0)=\sum_{E_0\leqslant E_\alpha\leqslant E_0+\Delta E_0}|c_m^\alpha|^2, \tag{11}$$

where the summation is performed over those unperturbed eigenstates that have an eigenenergy E_α in a fixed small energy interval $E_0\leqslant E_\alpha\leqslant E_0+\Delta E_0$, where for our computation ΔE_0 was taken to be $\Delta E_0=E_m/80$. For the state $|m\rangle$ considered in Fig. 12, ΔE_0 is roughly given by 1. One can see from Fig. 14 that a remarkable correspondence exists between the classical and quantum probability distributions of the delocalized EF's. This means that the weak localization of the delocalized EF's is a classical effect and is probably not related to quantum (dynamical) localization. This is in agreement with the previous result of Ref. [29].

IV. CONCLUSIONS

The main conclusion that can be reached from our investigation is that there exists a strong correspondence between quantum and classical descriptions of the Pullen-Edmond system. The strong localization of EF's can be explained by considering the corresponding classical motion on the KAM tori, and the weak localization of the delocalized EF's can be understood in terms of the corresponding classical probability distribution. There is no trace of quantum dynamical localization in the autonomous Hamiltonian system being considered.

One of the main issues of the quantum chaos research carried out recently on conservative systems is the structure of EF's. In this paper we investigated the relation between the localization of LSDS and that of EF's by considering the unitary matrix U that diagonalizes the Hamiltonian of the system. In our model system the localization of LSDS can be explained by considering the Hamiltonian structure. The off-diagonal components of H have a typical periodic structure [Fig. 2(b)]; they are small at the edges of each subgroup of eigenstates, while they are large at the middle of each subgroup. One can see from Fig. 5 that the unperturbed eigenstates corresponding to the edges of each subgroup also have a large L_{IPR} (which means strong localization), while the unperturbed eigenstates corresponding to the middle of each subgroup have a small L_{IPR} (which means delocalization or weak localization). An unperturbed eigenstate having small off-diagonal components can be nearly isolated from other states. It thus exhibits a strong localization and has a large L_{IPR}. The structure of the off-diagonal components of the Hamiltonian considered in the present work is strongly different from that of the conventional BRM where off-diagonal matrix components are randomly chosen or have the same value. The nonuniform structure of the off-diagonal components possesses information on the mixed type dynamics (KAM tori and chaotic region) of its classical counterpart. Therefore, the classical dynamics, the Hamiltonian structure (especially the structure of the off-diagonal components), and the structure of EF's are closely related to one another, which leads to the strong quantum-classical correspondence observed in this work for both localized and delocalized EF's.

ACKNOWLEDGMENTS

S. W. Kim thanks, with pleasure, Professor E. J. Heller and the colleagues of his group, especially Dr. L. Kaplan, of Harvard University, for their hospitality during his visit when a part of this work was done. This research was supported by the Ministry of Science and Technology of Korea under the project ''High Performance Computing-Computational Science and Engineering'' (HPC-COSE), and by the Agency for Defense Development (ADD) of Korea.

[1] L.E. Reichl, *The Transition to Chaos in Conservative Classical Systems: Quantum Manifestations* (Springer-Verlag, New York, 1992).
[2] M.C. Gutzwiller, *Chaos in Classical and Quantum Mechanics* (Springer-Verlag, New York, 1990).
[3] *Quantum Chaos between Order and Disorder* (Cambridge University Press, Cambridge, 1995), edited by G. Casati and B.V. Chirikov.
[4] G. Casati, B.V. Chirikov, F.M. Izrailev, and J. Ford, in *Stochastic Behavior in Classical and Quantum Hamiltonian Systems*, edited by G. Casati and J. Ford, Lecture Notes in Physics Vol. 93(Springer Verlag, Berlin, 1979), p. 334.
[5] S. Fishman, D.R. Grempel, and R.E. Prange, Phys. Rev. Lett. **49**, 509 (1982).
[6] G. Casati, B.V. Chirikov, and D.L. Shepelyansky, Phys. Rev. Lett. **53**, 2525 (1984).
[7] G. Casati, B.V. Chirikov, I. Guarneri, and D.L. Shepelyansky, Phys. Rev. Lett. **59**, 2927 (1987).
[8] E.J. Galvez, B.E. Sauer, L. Moorman, P.M. Koch, and D. Richards, Phys. Rev. Lett. **61**, 2011 (1988).
[9] J.E. Bayfield, G. Casati, I. Guarneri, and D.W. Sokol, Phys. Rev. Lett. **63**, 364 (1989).
[10] M. Arndt, A. Buchleitner, R.N. Mantegna, and H. Walther, Phys. Rev. Lett. **67**, 2435 (1991).
[11] R. Graham, M. Schlautmann, and P. Zoller, Phys. Rev. A **45**, R19 (1992).
[12] F.L. Moore, J.C. Robinson, C.F. Bharucha, P.E. Williams, and M.G. Raizen, Phys. Rev. Lett. **73**, 2974 (1994).
[13] P.J. Bardroff, I. Bialyniki-Birula, D.S. Krähmer, G. Kurizki, E. Mayr, P. Stifter, and W.P. Schleich, Phys. Rev. Lett. **74**, 3959 (1995).
[14] J.C. Robinson, C. Bharucha, F.L. Moore, R. Jahnke, G.A. Georgakis, Q. Niu, and M.G. Raizen, Phys. Rev. Lett. **74**, 3963 (1995).
[15] F. Borgonovi, G. Casati, and B. Li, Phys. Rev. Lett. **77**, 4744 (1996).

[16] L. Kaplan and E.J. Heller, Physica D **121**, 1 (1998).
[17] T. Guhr, A. Müller-Groeling, and H.A. Weidenmüller, Phys. Rep. **299**, 189 (1998).
[18] Y.V. Fyodorov and A.D. Mirlin, Phys. Rev. Lett. **67**, 2405 (1991).
[19] Y.V. Fyodorov and A.D. Mirlin, Int. J. Mod. Phys. B **8**, 3795 (1994).
[20] G. Casati, B.V. Chirikov, I. Guarneri, and F.M. Izrailev, Phys. Lett. A **223**, 430 (1996).
[21] I.C. Percival, J. Phys. B **6**, L229 (1973).
[22] B. Li and M. Robnik, J. Phys. A **28**, 2799 (1995).
[23] G. Carlo, E. Vergini, and A.J. Fendrik, e-print chao-dyn/9804016, 1998 (unpublished).
[24] O. Bohigas, S. Tomsovic, and D. Ullmo, Phys. Rep. **223**, 43 (1993).
[25] R.A. Pullen and A.R. Edmonds, J. Phys. A **14**, L477 (1981).
[26] In this work we use the term ''weak localization'' to signify that EF's having a small L_{IPR} are not completely delocalized. In some earlier investigations this term was used to denote quantum enhancement in the autocorrelation function of wave packet due to constructive interference of time-reversed paths.
[27] H.-D. Meyer, J. Chem. Phys. **84**, 3147 (1986).
[28] M. Tinkham, *Group Theory and Quantum Mechanics* (McGraw-Hill, New York, 1964).
[29] F. Borgonovi, I. Guarneri, and F.M. Izrailev, Phys. Rev. E **57**, 5291 (1998).
[30] R.J. Glauber, in *Quantum Optics and Electronics,* edited by C. Dewitt, A. Blandin, and C. Cohen-Tannoudji (Gordon and Breach, New York, 1965).
[31] H.-W. Lee, Phys. Rep. **259**, 147 (1995).
[32] Considering the RMT, we expect c_m^α to be Gaussian variables with the normalization condition $\Sigma c_m^\alpha = 1$. It leads to $L_{\mathrm{IPR}} = F$, where $F = 3$ if c_m^α is real (for the system having time-reversal symmetry), and $F = 2$ otherwise. This is a quantum fluctuation result and is a deviation from the classical expectation of $F = 1$ [34].
[33] O. Bohigas, M.-J. Giannoni, and C. Schmit, Phys. Rev. Lett. **52**, 1 (1984).
[34] L. Kaplan and E.J. Heller, Ann. Phys. (N.Y.) **264**, 171 (1998).